

The role of ADC histogram analysis in the diagnosis of pediatric malignant lymphadenopathy

 Turgut Seber¹,  Tuğba Uylar Seber¹,  Elif Aktaş¹,  Fatma Türkan Mutlu²,  Veysel Gök²,
 Şuayip Keskin³,  Fatoş Tekelioğlu⁴,  Erdem Arzu Taşdemir⁴

¹Department of Radiology, Kayseri City Education and Research Hospital, Kayseri, Turkey

²Department of Pediatric Hematology and Oncology, Kayseri City Education and Research Hospital, Kayseri, Turkey

³Department of Pediatric Health and Diseases, Kayseri City Education and Research Hospital, Kayseri, Turkey

⁴Department of Medical Pathology, Kayseri City Education and Research Hospital, Kayseri, Turkey

Cite this article as: Seber T, Uylar Seber T, Aktaş E, et al. The role of ADC histogram analysis in the diagnosis of pediatric malignant lymphadenopathy. *Anatolian Curr Med J* 2023; 5(2); 91-96.

ABSTRACT

Aim: Lymphadenopathy (LAP) is one of the most common daily practice clinical findings in children. LAPs that involve more than one region and do not decrease with treatment are a significant cause of anxiety for clinicians and families. In this occurrence, ultrasonography, which is the primary imaging method, is insufficient in some cases. Our aim is to make histopathological predictions with apparent diffusion coefficient (ADC) histogram analysis.

Material and Method: A total of thirty-one patients, seventeen male and fourteen female, who underwent magnetic resonance imaging and were diagnosed histopathologically (with tru-cut or excisional biopsy) were included in our study. Magnetic resonance imagings were evaluated retrospectively.

Results: We could not differentiate lymphoma (when considered as a single group), granulomatous LAP and reactive lymphoid hyperplasia with an ADC histogram analysis ($p>0.05$). However, when the lymphoma subgroups were evaluated separately, we could only distinguish Burkitt's lymphoma (with ADCmin values) from other pathologies ($p<0.05$). The optimal cut-off value distinguishing Burkitt's lymphoma from other groups was $245 \times 10^{-6} \text{ mm}^2/\text{sec}$ in receiver operating characteristic curve analysis (AUC 0.981, sensitivity 75%, specificity 93%, PPV 67%, NPV 93%). As in recent studies, we did not find significant differences in ADC histogram analysis values of reactive lymphoid hyperplasia, granulomatous LAPs and lymphomas (when considered as a single group). However, when the lymphoma subgroups were considered separately, we were able to distinguish Burkitt's lymphoma from other subgroups and granulomatous LAP, reactive lymphoid hyperplasia with the ADCmin value.

Conclusion: The ADCmin value in pediatric LAPs may contribute to the diagnosis of Burkitt's lymphoma.

Keywords: Lymphadenopathy, pediatric, magnetic resonance imaging, histogram analysis, apparent diffusion coefficient

INTRODUCTION

Lymphadenopathy (LAP) is a common clinical finding in children and results from the infiltration in lymph nodes with phagocytic or malignant cells or the proliferation of normal lymphoid elements. In most patients, the cause can be identified with a careful history and a complete physical examination. Since infections are the most common cause, the majority of children are given empirical antibiotic therapy first (1). If the lymph nodes do not regress in size or if they increase in size and number within 4 to 6 weeks, and there are systemic complaints, laboratory and imaging methods are used to determine the underlying cause (2). Ultrasound is the most suitable initial imaging method, as it does not contain ionizing radiation. Computed tomography and magnetic resonance imaging (MRI) are usually complementary and contribute to the diagnosis when required.

It has been reported that diffusion-weighted imaging (DWI) is effective in distinguishing benign and malignant lymph nodes, and can help conventional sequences (3, 4). Our aim was to minimize data loss with apparent diffusion coefficient (ADC) map histogram analysis (HA) and to prevent individual-dependent subjective assessment (5, 6).

MATERIAL AND METHOD

The study was carried out with the permission of Kayseri City Hospital Clinical Researches Ethics Committee (Date: 29.09.2022, Decision No: 706). All procedures were carried out in accordance with the ethical rules and the principles of the Declaration of Helsinki.

Thirty-one children were retrospectively re-evaluated, between December 2019 and January 2022. We obtained the clinical information and MRIs of the subjects from the hospital records and the PACS system.

Study Patients

The patients consisted of seventeen boys and fourteen girls, with a mean age of thirteen years and a range of 4 to 17. All subjects were undergoing MRI and diagnosed histopathologically with tru-cut or excisional biopsy.

MRI Technique

All MRI examinations were performed on a 3T MRI (Magneatom Skyra; Siemens Healthcare, Erlangen, Germany) using a body matrix 8-channels flex coil and 20 channels neck coil, depending on the localization of lymph nodes. Intravenous sedation (ketamine 1 mg/kg) was performed for two children who were six and seven years old, in order to prevent motion artifacts. All subjects had standard sequences (including T1 and T2 weighted turbo spin-echo, contrast-enhanced T1 turbo spin-echo) with DWI and ADC map. Interleaved multi-shot (IMS) echo-planar imaging (EPI) DWI sequences were acquired using 2 b values ($b=0-1000 \text{ sec/mm}^2$) and 3 orthogonal (x, y, z) diffusion directions. ADC was the mean diffusivity. The acquisition parameters of DWI were as follows: FOV=120×120 mm; matrix size 128×128; slice thickness=4 mm; voxel size=0.9×0.9×4 mm; distance factor=0%; TR=6600 msn; TE=87 msn; turbo factor=128; number of excitations=3; integrated parallel acquisition technique factor=2. ADC maps were pixel-based and postprocessed, with a mono-exponential calculation from DWI.

Imaging Evaluation

Volumetric HA was performed for lymph nodes on the ADC map. Lymph nodes were drawn separately in each slice with a free-hand 3D volume of interest. Necrotic areas were excluded from the volume of interest. The quantitative ADC values (mean [ADC_{mean}], median [ADC_{median}], mode [ADC_{mode}], minimum [ADC_{min}], maximum [ADC_{max}], kurtosis, skewness, P10 [10th percentile ADC], P25 [25th percentile ADC], P75 [75th percentile ADC], P90 [90th percentile ADC]) were obtained separately for each region and statistically compared with the histopathology. Analyses and evaluations were performed on a Syngo Via (Software Version VA30A, Siemens AG, Germany) Workstation by a pediatric radiologist (T.S.) with seven years of experience in pediatric radiology.

Statistical Analyses

The distribution of histogram parameters was normal with the “Kolmogorov–Smirnov” test. The “One Way Anova” test was used to compare each parameter with the histopathology in the groups. Receiver operating characteristic (ROC) curve analyses were used to

determine the potential diagnostic performance. All statistical analyses were performed using the SPSS software (version 22.0; SPSS Inc., Chicago, IL, USA). In all analysis, $p<0.05$ was taken to indicate statistical significance.

RESULTS

The study population consisted of thirty-one patients (seventeen boys and fourteen girls, age range of 4 to 17 years, with a mean age of 13 years). There were no significant differences in sex or age distribution between the groups ($p=0.5$ and $p=0.8$, respectively).

Histopathological diagnoses of LAPs are reactive lymphoid hyperplasia ($n=7$), granulomatous LAP (GL) ($n=7$), nodular sclerosing HL ($n=5$), Burkitt's lymphoma (BL) ($n=4$), anaplastic large cell NHL ($n=4$) and mixed cellular HL ($n=4$).

With HA, the differentiation of lymphoma (when considered as a single group), GL and RLH was not statistically significant ($p>0.05$). When lymphoma subgroups were considered separately, only the ADC_{min} values of BL were found to be significantly lower than other pathologies (Table 1, Figure 1). The optimal cut-off value distinguishing BL from other groups was $245 \times 10^{-6} \text{ mm}^2/\text{sec}$ in ROC curve analysis (AUC 0.981, sensitivity 75%, specificity 93%, PPV 67%, NPV 93%) (Figure 2). The long and short axis of lymph nodes were significantly larger in lymphoma compared to other groups ($p=0.005$), and there was no significant difference between RLH and GL ($p=0.13$) (Table 2, Figure 3). Cut-off values distinguishing lymphoma from other groups were 31 mm for the long axis (AUC 0.899, sensitivity 88%, specificity 86%, PPV 88%, NPV 86%), 21.5 mm for the short axis in ROC curve analysis (AUC 0.868, sensitivity 82%, specificity 79%, PPV 87%, NPV 80%) (Figure 4).

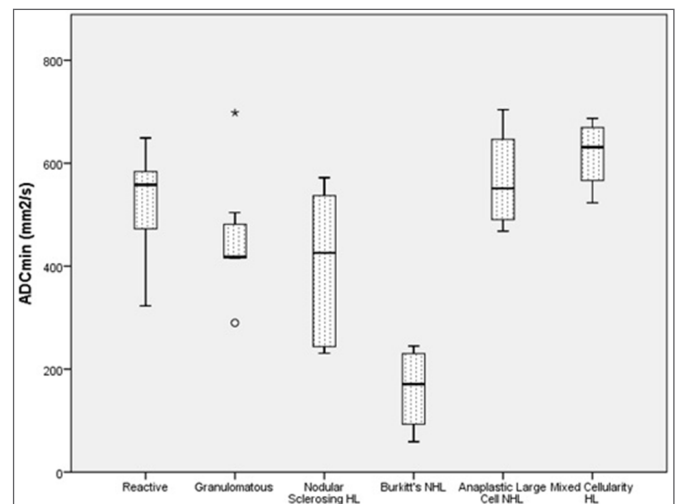


Figure 1. Box- and- Whisker plot showing the distribution of groups according to ADC_{min}

(ADC apparent diffusion coefficient, HL Hodgkin's lymphoma, Min minimum, NHL non-Hodgkin's lymphoma)

Table 1. Distribution of histopathologies according to ADCmin values

Histopathology	N (%)	Mean±SD	Min.-Max.	95% CI	P value (differentiation from Burkitt's Lymphoma)
Reactive LH	7 (22.6%)	520±112	323-649	416-624	0.001
Granulomatous LAP	7 (22.6%)	457±124	290-698	342-572	0.005
Nodular Sclerosing HL	5 (16.1%)	402±159	231-572	231-600	0.05
Burkitt's Lymphoma	4 (12.9%)	161±84	59-245	59-245	-----
Anaplastik Large cell NHL	4 (12.9%)	568±103	468-704	468-704	0.001
Mixed Cellularity HL	4 (12.9%)	618±70	523-687	523-687	0.001
Total	31(100%)				

(ADC apparent diffusion coefficient, HL Hodgkin's lymphoma, LAP lymphadenopathy, LH lymphoid hyperplasia Max maximum, Min minimum, N number of cases, NHL non-Hodgkin's lymphoma, SD standard deviation; The unit of values is 10⁻⁶×mm²/sec)

Table 2. Shows the distribution of the short and long axes of the lymph nodes according to the groups

Histopathology	N (%)	Short axis	Long axis
		Min.-Max. (Mean±SD) [95% CI]	Min.-Max. (Mean±SD) [95% CI]
Reactive LH	7 (22.6%)	5 – 14 mm (8.43±2.99) [5.66 – 11.2]	10 – 22 mm (14.43±4.27) [10.47 – 18.38]
Granulomatous LAP	7 (22.6%)	6 – 35 mm (19.14±10.97) [8.99 – 29.29]	10 – 51 mm (27.14±16.32) [12.05 – 42.24]
Nodular Sclerosing HL	5 (16.1%)	19 – 60 mm (39±17.29) [17.53 – 60.47]	32 – 74 mm (53±16.88) [32.04 – 73.96]
Burkitt's Lymphoma	4 (12.9%)	22 – 42 mm (29±9.45) [13.96 – 44.04]	33 – 55 mm (40.25±10.04) [24.27 – 56.23]
Anaplastik Large cell NHL	4 (12.9%)	21 -33 mm (26.5±5.19) [18.23 – 34.77]	30 -54 mm (39.5±10.24) [23.19 – 55.81]
Mixed Cellularity HL	4 (12.9%)	16 – 43 mm (29.25±11.5) [10.95 – 47.55]	27 – 67 mm (43.5±17.13) [16.23 – 70.77]
Total	31 (100%)		

(CI confidence interval, HL Hodgkin's lymphoma, LAP lymphadenopathy, LH lymphoid hyperplasia, Max maximum, Min minimum, NHL non-Hodgkin's lymphoma, SD standard deviation)

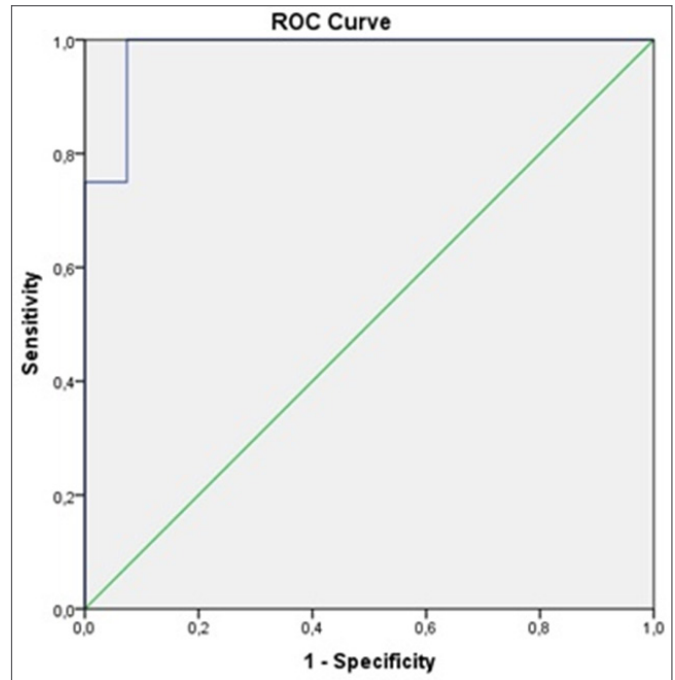


Figure 2. ROC curve analysis showing the differentiation of Burkitt's lymphoma from other lymphoma subgroups and pathologies according to ADCmin values. (ADC apparent diffusion coefficient, Min minimum)

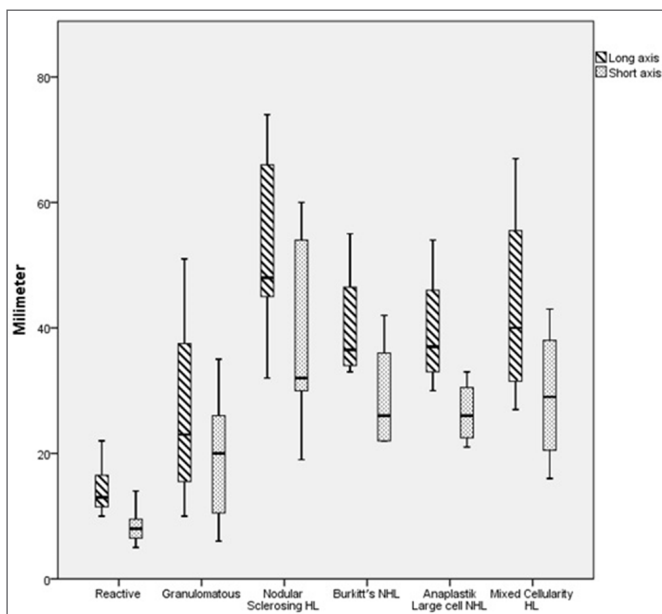


Figure 3. Box and Whisker plot graph showing the distribution of the groups according to the short and long axes (HL Hodgkin's lymphoma, NHL non-Hodgkin's lymphoma)

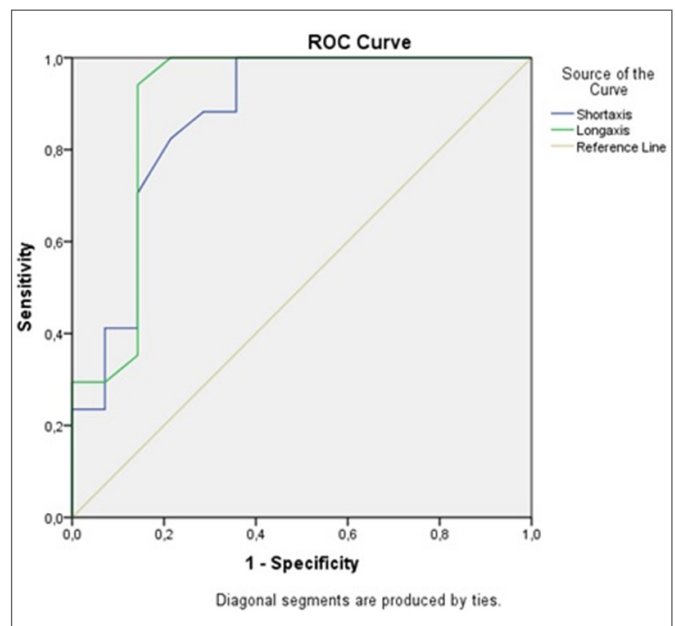


Figure 4. ROC curve analysis showing the differentiation of lymphoma from other groups according to the short and long axes of the lymph nodes

DISCUSSION

DWI visualizes the differences in movement of water between cells in the tissues. Cellular tissues (e.g., lymph nodes) give a high signal, while less cellular tissues have a low signal. Thus, lymph nodes can be easily distinguished from the surrounding tissues. Diffusion can be measured by the ADC map obtained from DWI, which allows tissue characterization and is easily reproducible (7-9). Clinicians can easily identify possible causes of LAP by history and physical examination and rarely require imaging. In these situations, it is crucial for the radiologist to recognize the normal cervical lymph nodes, and report nodal features of specific infections, inflammatory conditions and neoplasms, to assist clinicians in treatment.

RLH is a benign nodular lesion histopathologically characterized by marked proliferation of non-neoplastic polyclonal lymphocytes, that form follicles with active germinal centers. GL is divided into infectious and non-infectious (10). Infectious GL is divided into suppurative and non-suppurative. The suppurative type was not included in our study because it contained central abscess or necrosis (**Figure 5**). The non-infectious type mostly consists of berylliosis, sarcoidosis and sarcoidosis-like reactions (11). In this type, central abscess or necrosis is very rare and is usually caused by tuberculosis and Bacillus Calmette-Guerin (BCG) lymphadenitis. Low ADC values, which can be confused with malignancy, can be observed in RLH and GL (4,12-14).

Studies of ADC-HA in lymph nodes have generally been performed on adults and are aimed at differentiating lymphoma from squamous cell carcinoma metastasis (5,15) and nasopharyngeal carcinoma (16,17). Our study, for its part, was carried out in children with no known diseases and isolated LAP in different body parts, which we meet frequently in our daily practice. We did not have a patient with a diagnosis of squamous cell carcinoma. Therefore, he is not in our study group.

Lymphoma constitutes 10 to 15% of all childhood malignancies. There are two types, HL and NHL: the latter is more common and BL is the most common subtype of NHL in children (40%), whereas it is the least subtype in adults (**Figures 6** and **7**). The sporadic variant is associated with abdominal involvement (18,19). It can be localized or has a diffuse infiltrative pattern. It is an aggressive tumor with a doubling time of 24 to 48 hours. Therefore, early diagnosis and treatment are life-saving (airway obstruction and spinal cord compression are important causes of mortality and morbidity). MRI is very valuable in diagnosis because of its high soft tissue contrast. DWI makes a significant contribution to conventional sequences in the diagnosis of lymphoma (20).

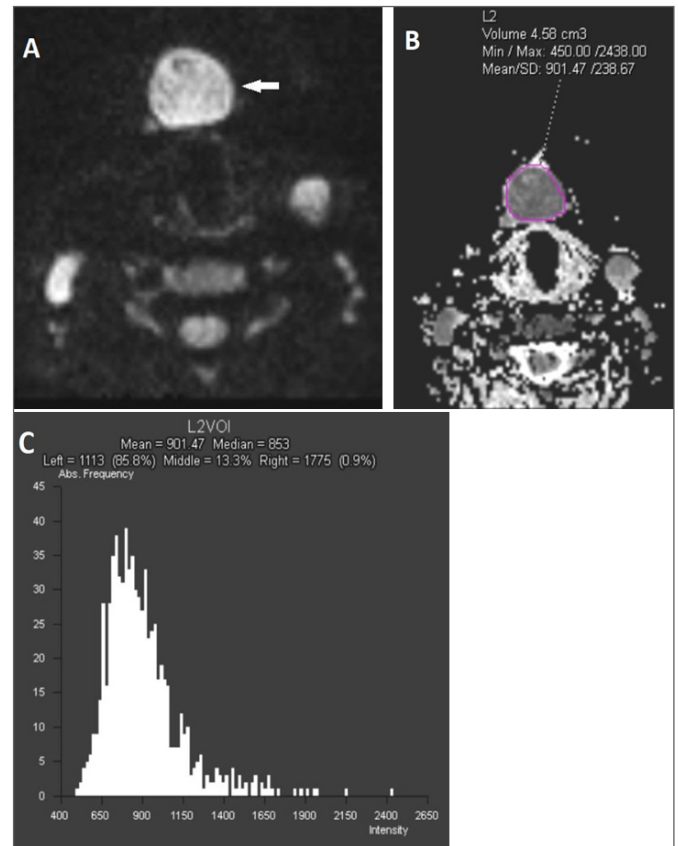


Figure 5. A 15-year-old girl had a lymphadenopathy (arrow) in the submental region (level 1A) that did not decrease in size with treatment (DWI [A], ADC map [B]). Histogram plot (C) was obtained from the lymphadenopathy. Histopathological result was consistent with granulomatous lymphadenopathy.

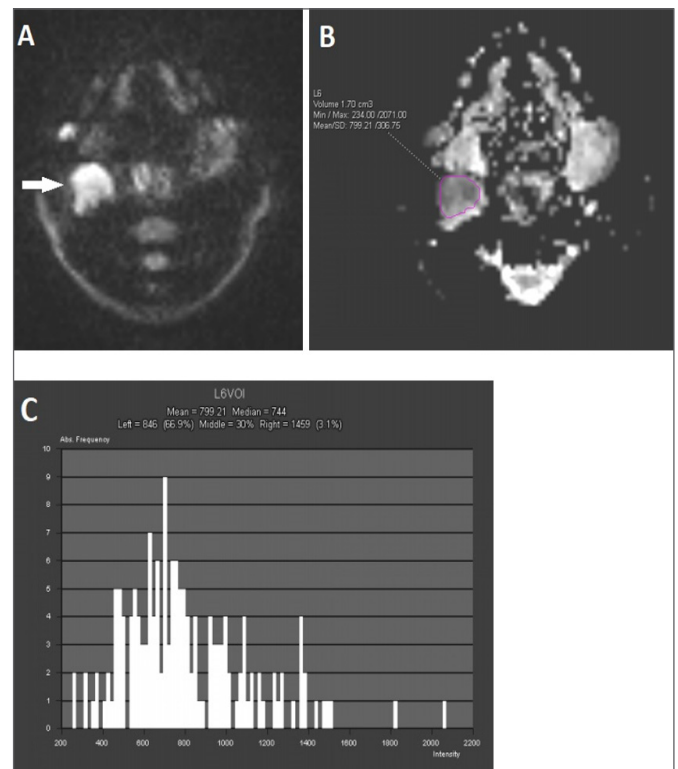


Figure 7. 10-year-old boy had a lymphadenopathy (arrow) with diffusion restriction (DWI [A], ADC map [B]) in the right submandibular region (level 2A). Histogram plot (C) was obtained from the lymphadenopathy. Histopathological result was consistent with Burkitt's lymphoma.

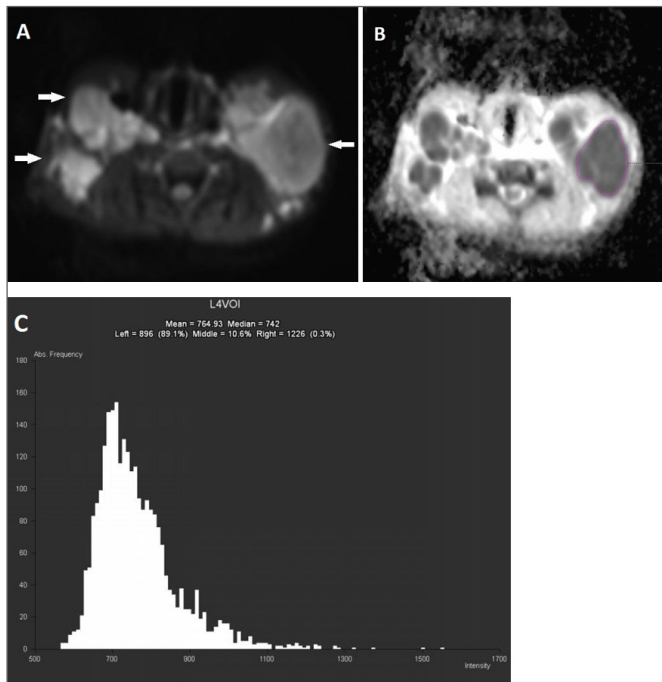


Figure 6. 13-year-old boy had multiple lymphadenopathies (arrows) with diffusion restrictions (DWI [A], ADC map [B]) in the bilateral anterior-posterior cervical chain (level 4-5B). Histogram plot (C) was obtained from large lymphadenopathy at left level 5B. Histopathological result was consistent with classical HL (nodular sclerosing type).

Early studies of DWI in lymph nodes reported significant differences in mean ADC values between lymphoma and normal lymph nodes (3,21-23). However, subsequent studies have found that mean ADC values overlap in pathological and normal lymph nodes (24,25). In some studies about mediastinal lymph nodes, ADC values were found to be significantly lower in lymphoma than in sarcoidosis (26,27). Differentiation of lymphoma subgroups (NHL, HL) could not be achieved in most studies (14,28,29). In these studies, only mean, min and max ADC values were obtained without HA. As in recent studies, we found no significant differences in the ADC-HA of RLH, GLs and lymphomas. However, when the subgroups of lymphoma were considered separately, we were able to distinguish BL from other subgroups and GL, RLH via the ADCmin value. ADCmin values of BL were found to be significantly lower than other pathologies.

CONCLUSION

ADCmin value in pediatric LAPs may contribute to the diagnosis of BL.

ETHICAL DECLARATIONS

Ethics Committee Approval: The study was carried out with the permission of Kayseri City Hospital Clinical Researches Ethics Committee (Date: 29.09.2022, Decision No: 706).

Informed Consent: Because the study was designed retrospectively, no written informed consent form was obtained from patients.

Referee Evaluation Process: Externally peer-reviewed.

Conflict of Interest Statement: The authors have no conflicts of interest to declare.

Financial Disclosure: The authors declared that this study has received no financial support.

Author Contributions: All of the authors declare that they have all participated in the design, execution, and analysis of the paper and that they have approved the final version.

Acknowledgements: We would like to thank the Medical Specialty Education Committee for their permission. The English in this document has been checked by J.Y.B, who is native English speaker and professional editor. We thank him for his contributions.

REFERENCES

- Nield LS, Kamat D. Lymphadenopathy in children: when and how to evaluate. *Clin Pediatr (Phila)* 2004; 43: 25-33.
- Tower RL, Carmitta BM. Lymphadenopathy. In: Kliegman RM, Stanton BF, St Geme JW, Schor NF (eds). *Nelson Textbook of Pediatrics* (20th ed). California, 2016: 2413-15.
- Abdel Razeq AA, Soliman NY, Elkhamary S, Alsharaway ML, Tawfik A. Role of diffusionweighted MR imaging in cervical lymphadenopathy. *Eur Radiol* 2006; 16: 1468-77.
- Vandecaveye V, De Keyzer F, Vander Pooten V, et al. Head and neck squamous cell carcinoma: value of diffusion-weighted MR imaging for nodal staging. *Radiology* 2009; 251: 134-46.
- Wang YJ, Xu XQ, Hu H, et al. Histogram analysis of apparent diffusion coefficient maps for the differentiation between lymphoma and metastatic lymph nodes of squamous cell carcinoma in head and neck region. *Acta Radiol* 2018; 59: 672-80.
- De Paepe KN, De Keyzer F, Wolter P, et al. Improving lymph node characterization in staging malignant lymphoma using first-order ADC texture analysis from whole-body diffusion-weighted MRI. *J Magn Reson Imaging* 2018; 48: 897-906.
- Le Bihan D. Molecular diffusion nuclear magnetic resonance imaging. *Magn Reson Q* 1991; 7: 1-30.
- Koh DM, Collins DJ. Diffusion-weighted MRI in the body: applications and challenges in oncology. *AJR Am J Roentgenol* 2007; 188: 1622-35.
- Donners R, Blackledge M, Tunariu N, Messiou C, Merkle EM, Koh DM. Quantitative whole-body diffusion-weighted MR imaging. *Magn Reson Imaging Clin N Am* 2018; 26: 479-94.
- Chang KL, Arber DA, Gaal KK, Weiss LM. Lymph nodes and spleen. In: Silverberg SG, DeLellis RA, Frable WJ, LiVolsi VA, Wick MR, editors. *Silverberg's Principles and practice of surgical pathology and cytopathology*. Volume 1. New York: Churchill Livingstone; 2006: 507-607
- Brincker H. Sarcoid reactions in malignant tumours. *Cancer Treat Rev* 1986; 13: 147-56.
- ElSaid NA, Nada OM, Habib YS, et al. Diagnostic accuracy of diffusion weighted MRI in cervical lymphadenopathy cases correlated with pathology results. *Egypt J Radiol Nuclear Med* 2014; 45: 1115-25.

13. Nomori H, Mori T, Ikeda K, et al. Diffusion-weighted magnetic resonance imaging can be used in place of positron emission tomography for N staging of nonsmall cell lung cancer with fewer false-positive results. *J Thorac Cardiovasc Surg* 2008; 135: 816-22.
14. Abdel Razek AA, Gaballa G, Elashry R, Elkhamary S. Diffusion-weighted MR imaging of mediastinal lymphadenopathy in children. *Jpn J Radiol* 2015; 33: 449-54.
15. Vidiri A, Minosse S, Piludu F, et al. Cervical lymphadenopathy: can the histogram analysis of apparent diffusion coefficient help to differentiate between lymphoma and squamous cell carcinoma in patients with unknown clinical primary tumor? *Radiol Med* 2019; 124: 19-26.
16. Lian S, Zhang C, Chi J, Huang Y, Shi F, Xie C. Differentiation between nasopharyngeal carcinoma and lymphoma at the primary site using whole-tumor histogram analysis of apparent diffusion coefficient maps. *Radiol Med* 2020; 125: 647-53.
17. Song C, Cheng P, Cheng J, Zhang Y, Xie S. Value of apparent diffusion coefficient histogram analysis in the differential diagnosis of nasopharyngeal lymphoma and nasopharyngeal carcinoma based on readout-segmented diffusion-weighted imaging. *Front Oncol* 2021; 11: 632796.
18. Molyneux EM, Rochford R, Griffin B, et al. Burkitt's lymphoma. *Lancet* 2012; 379: 1234-44.
19. Thomas AG, Vaidhyanath R, Kirke R, Rajesh A. Extranodal lymphoma from head to toe: part 1, the head and spine. *AJR Am J Roentgenol* 2011; 197: 350-6.
20. Gu J, Chan T, Zhang J, Leung AY, Kwong YL, Khong PL. Whole-body diffusion-weighted imaging: the added value to whole-body MRI at initial diagnosis of lymphoma. *AJR Am J Roentgenol* 2011; 197: W384-91.
21. Kwee TC, Ludwig I, Uiterwaal CS, et al. ADC measurements in the evaluation of lymph nodes in patients with non-Hodgkin lymphoma: feasibility study. *MAGMA* 2011; 24: 1-8.
22. Holzapfel K, Duetsch S, Fauser C, Eiber M, Rummeny EJ, Gaa J. Value of diffusion-weighted MR imaging in the differentiation between benign and malignant cervical lymph nodes. *Eur J Radiol* 2009; 72: 381-7.
23. Perrone A, Guerrisi P, Izzo L, et al. Diffusion-weighted MRI in cervical lymph nodes: differentiation between benign and malignant lesions. *Eur J Radiol* 2011; 77: 281-6.
24. De Paepe K, Bevernage C, De Keyzer F, et al. Whole-body diffusion-weighted magnetic resonance imaging at 3 Tesla for early assessment of treatment response in non-Hodgkin lymphoma: a pilot study. *Cancer Imaging* 2013; 13: 53-62.
25. Wu X, Nerisho S, Dastidar P, et al. Comparison of different MRI sequences in lesion detection and early response evaluation of diffuse large B-cell lymphoma--a whole-body MRI and diffusion-weighted imaging study. *NMR Biomed* 2013; 26: 1186-94.
26. Santos FS, Verma N, Marchiori E, et al. MRI-based differentiation between lymphoma and sarcoidosis in mediastinal lymph nodes. *J Bras Pneumol* 2021; 47: e20200055.
27. Sabri YY, Kolta MFF, Khairy MA. MR diffusion imaging in mediastinal masses the differentiation between benign and malignant lesions. *Egypt J Radiol Nucl Med* 2017; 48: 569-80.
28. Sabri YY, Nossair EZB, Assal HH et al. Role of diffusion weighted MR-imaging in the evaluation of malignant mediastinal lesions. *Egypt J Radiol Nucl Med* 2020; 51: 1-16.
29. Sabri YY, Ewis NM, Zawam HE, Khairy MA. Role of diffusion MRI in diagnosis of mediastinal lymphoma: initial assessment and response to therapy. *Egyptian Journal of Radiology and Nuclear Medicine* 2021; 52: 1-11.